High Shear Dispersion Technology prior to Twin Roll Casting for High Performance Magnesium/SiC_p Metal Matrix Composite Strip Fabrication

Xinliang Yang[1], Yan Huang[1], Nilam S. Barekar[1], Sanjeev Das[2], Ian C. Stone[1] and Zhongyun Fan[1]

[1]BCAST, Brunel University London, Uxbridge, UB8 3PH, UK

[2]Department of Metallurgical Engineering, National Institute of Technology Raipur, G.E. Road, Chhattisgarh, 492010, India

Abstract: SiC particulate (SiC_p) reinforced AZ31 magnesium alloy composite strips were produced by a novel process. In the process, a high shear technique was utilised to disperse the reinforcing particles uniformly into the matrix alloy, and AZ31/5vol%SiC_p slurry was solidified into thin strip by a horizontal twin roll caster. The experimental results showed that the AZ31/5vol%SiC_p strip obtained with high shear treatment exhibited a significantly refined microstructure and uniform distribution of reinforcing SiC particles. High cooling rate in the TRC process was also considered to contribute to the grain refinement of the matrix alloy, together with the possible heterogeneous nucleation effect of the reinforcing particles. The mechanical properties of the high shear treated composites strips showed enhanced modulus, yield strength and ductility by hardness and tensile tests. The experimental results were discussed in terms of the microstructural features and the macroscopic reliability, where necessary, analytical and statistical analyses were conducted.

Keywords:

A. Metal-matrix composites (MMCs); B. Microstructure, Mechanical properties; E. Twin roll casting (TRC)

1. Introduction

Magnesium alloys have found a wide range of applications in transport and 3C (Computers, Communications and Consumer-electronics) industries due to their low density, high specific strength, and excellent heat dissipation, electromagnetic shielding and vibration damping capacity. However, their actual use in automobile industry has been stagnated in the last decade or so, although they have shown a great potential in manufacturing lightweight structures for vehicles to enhance fuel efficiency and reduce carbon footprints. A key factor limiting the application of magnesium alloys for vehicle body structures is their poor absolute strength [1]. In recent years, extensive investigations have been carried out for developing high strength magnesium alloys with various combinations of alloying elements and strengthening mechanisms [2-4]. An alternative solution is the development of magnesium metal matrix composites (Mg-MMC) reinforced with ceramic fibres, whiskers and particles. From the standpoint of isotropic mechanical properties, particulate reinforced magnesium matrix composites are mostly studied [5-7].

A critical challenge for fabricating Mg-MMC, as for any other types of MMCs, is to overcome severe agglomeration of the reinforcing particles which act as stress concentration points. In powder metallurgy, ball milling and tumble blending [8] is normally used to mix the reinforcing particles with the matrix powder. For the casting route, mechanical stirring has been a routine method to mix the reinforcing particles in the molten matrix alloys [9]. The problem with conventional mechanical stirring is that the shear rate applied is inadequate to break up particle agglomerations, particularly when the reinforcing particle size is ultrafine (< 10 μm) and also high volume fraction [10]. The turbulence generated in the melt surface during mixing by conventional

mechanical stir is a main cause for the gas entrapment in the matrix melt [11]. In order to overcome the cohesive force of the clusters embedded in the liquid melt, a rotor-stator device has been developed at BCAST for melt conditioning by high shear technology. It generates high shear rate (up to ~10^6 s^{-1}) with minimum turbulence on the melt surface [12,13]. It has been shown that the application of the shear force can surpass the cohesive bonding of neighbour particles which dominates the agglomeration strength [14], and thus can effectively break up agglomerations, leading to a more uniform reinforcement distribution with improved interfacial wettability between the matrix and reinforcing particles.

Besides, the distribution of reinforcing particles is often dependent on the microstructure of the matrix alloy, particularly when the wetting between the particles and the matrix is limited [15]. This is because the particles tend to dwell along grain boundaries in the case of poor wetting between the particles and the matrix. In general, particles segregate more or less in grain boundaries. Therefore, a fine grain structure will give a better distribution of particles. Twin roll casting (TRC) process provides much higher cooling rate (~10^2 K/s) than most of the industrial casting processes [16], and is expected to produce a fine grain structure and improved reinforcing particle distribution. Additionally, MMCs in the form of strip/sheet as the product of TRC process has several advantages over bulk products for structural applications as it can be stamped into various shapes with higher freedom of design, although further investigations are required to make full use of these advantages [17,18].

The aim of present study was to investigate the influence of high shear technique on the distribution of reinforcing particles, matrix microstructure and mechanical properties of particulate reinforced magnesium matrix composite strips produced by twin roll casting.

2. Experimental procedure

2.1 Magnesium matrix composites synthesis

A commercial AZ31 (Mg-3.29Al-1.02Zn-0.386Mn, in wt%) magnesium alloy, supplied by Magnesium Elektron Ltd at Manchester, UK, was used as the matrix alloy and angular shaped SiC_p with an average particle size of 4.5 μm were selected as the reinforcing elements (Logitech Ltd, Glasgow, UK). The matrix alloy was melted at 680°C (T_{mAZ31} ~ 629°C) in a thermally controlled crucible, which was placed in semi-sealed mixing chamber under the protection of N_2+SF_6. The SiC_p were pre-heated in an oven at 400°C for 1 hour and were added to the AZ31 melt at 680°C immediately after the pre-heating. The mixing was conducted in two stages. Firstly, the SiC_p were introduced to the melt and mixed with the help of mechanical stirring using a 45° four-bladed impeller at 650 rpm for 5 minutes. Then the mixed AZ31 and SiC_p slurry was subjected to high shear treatment using a rotor-stator device. The rotor-stator device is consisted of a motor driven rotor with an impeller and an open cylinder stator with narrow apertures at its bottom section. During mixing, the impeller rotates at a high speed between 1000 – 10000 rpm, sucking the melt into the stator and forcing the melt through the narrow apertures and thus applying high shear rate to the melt [12,13]. The material flow is characterized by a continuous and turbulent convection [19]. In the present experiment, the high shear treatment was employed at a speed of 5000 rpm for 5 minutes and the composite slurry was kept at 680°C during shearing and was protected by the same N_2+SF_6 gas mixture. This high shear treated composite slurry was then cast into strip by using the twin roll caster. Such processed composite strip will be referred to as high shear (HS) strip in the following context. For comparison, AZ31/SiC_p composite strip was also produced using slurry subjected only to mechanical stir

without high shear treatment and is referred to as non-high shear (nonHS) strip. The two-stage mixing process (mechanical stirring and high shear treatment) and the TRC process are schematically shown in Figure 1.

2.2 TRC process for magnesium matrix composite

Twin roll casting (TRC) was carried out on an in-house-built horizontal twin-roll caster with an internal water circulation cooling system. The rolls were 100 mm in diameter with a working width of 150 mm and 5 m/min rolling speed. The AZ31/5vol%SiC_p slurry of about 4 kg prepared with or without high shear treatment was fed to the caster through a stainless steel tundish with composites slurry temperature of 650°C. The setback of tundish tip to the roll biting point was 20 mm. Again, protective gas mixture of 0.42% SF_6 in nitrogen was applied on the slurry surface to protect it from oxidation.

2.3 Homogenization

Prior to tensile testing, the as-cast strip was homogenized at 400°C for 48 hour in a heat treatment furnace with forced air circulation, in order to reduce chemical segregation and residual stresses in the materials and water quenched to retain the solute solution at the homogenization temperature.

2.4 Microstructural characterization

Samples for microstructural characterization were taken along the longitudinal section (TD plane) and transverse section (CD plane) through the middle of both HS and nonHS AZ31/5vol%SiC_p strip. For particle distribution analysis, five sets of samples were taken in the middle of composites strip, 500 mm apart from each other along the casting direction. Samples of 10×10 mm in square shape for X-ray diffraction (XRD) analysis were taken from the centre of the HS strip. Metallographic sample preparation was performed following the standard route with a final polish using a 0.05 µm oil base

alumina suspension. Ethanol solution with 5% HNO_3 was used as etchant for revealing AZ31 matrix morphology under optical microscope. For primary α-Mg grain size measurement, a solution of 4.2 g picric acid, 15 ml acetic acid, 70 ml ethanol and 15 ml distilled water was employed for colour etching. Samples for particle distribution analysis were not etched. The XRD analysis was conducted on a Bruker D8 Advance Cu-α target radiation on the polished sample surface. The optical microscopic observations were performed on a Carl Zeiss AxioScope A1 optical microscope. Secondary and backscatter electron imaging and EDS mapping was performed on a Zeiss Supra 35 field-emission gun SEM equipped with EDX detector (Oxford Instruments). The fracture features of the tensile samples were examined on the SEM immediately after tensile tests.

2.5 Mechanical properties tests

The tensile samples of both HS and nonHS AZ31/5vol%SiC_p strips were machined following the ASTM B557 standard with the gauge length of 50.00±0.10 mm along the strip casting direction. The tensile properties measurement was conducted with 5 samples of HS and nonHS strips on an Instron 5500 Universal Electromechanical Testing System with a constant cross head speed of 0.65mm/min (2×10^{-4} s^{-1} initial strain rate) and Bluehill software for test process control. All the tests were performed at ambient temperature (~25℃).

The hardness test were performed on a Buehler Micromet 5101 Vickers Hardness tester with a load of 0.5 kg and for a dwell time of 10 s. Samples for Vickers hardness test were taken from the longitudinal section of both the as-cast HS and nonHS strips with standard polishing process.

3. Results and discussion

3.1 General strip appearance and constituents

Under the prescribed experimental conditions, AZ31/5vol%SiC_p slurry exhibited sufficient fluidity and the TRC process was conducted smoothly. The strip thickness obtained was about ~1.7 mm, with limited variations along the strip width and length. The typical strip length with a uniform microstructure cast at stabilized process parameters was about 3 m, which was used for further processing and analysis. Fig. 2 shows a photograph of typical AZ31/5vol%SiC_p composite strip and it can be seen that the surface finish is reasonably good, although there are some fine cracks at the edge of the strip. Microstructural examinations confirmed that there were no defects such as bleeding [20] and cracking in the material apart from the fine cracks at the very edges of the strip. XRD analysis revealed that the constituents of the composite consisted mainly of, as expected, α-Mg phase, SiC reinforcement and $Mg_{17}Al_{12}$ intermetallic phase, which are corresponding to the peaks in the XRD spectrum in Fig. 3.

3.2 SiC_p distribution

Figure 4 shows the optical micrographs obtained from both the TD and CD sections of both the HS and nonHS strips in the as-cast state, in which SiC particles appear as the dark phase. It can be seen from Figure 4(b) that the composite strip subjected to only mechanical stir prior to TRC exhibited severe particle agglomerations in the form of variously sized clusters and some area of several hundred microns. The particle clusters are elongated along the casting direction, corresponding to the material flow due to plastic deformation during TRC. Severe particle agglomeration resulted in large amount of areas which are either depleted or free from reinforcing particles. On the other hand, the composite strip subjected to both mechanical stir and high shear treatment displayed a globally uniform particle distribution within the matrix alloy and with substantially

reduced agglomerations. As shown in the Figure 4(a), the reinforcing SiC particles are spread evenly over both the TD and CD planes throughout the strip thickness. Microstructure examination showed that such particle distribution features remained consistent over the full strip length obtained under steady state TRC. A critical problem for twin roll casting of magnesium alloy and most other alloys is the formation of central line segregation consisting of solute rich phases, which is primarily due to the directional columnar growth of primary α-Mg phase from the surface towards the centre [20]. In the present work, no columnar structures for both the HS and nonHS composite strips were observed and variations of reinforcing particle volume fraction and of chemical compositions through the strip thickness were limited for HS strip. Previous studies on melt conditioned magnesium alloys suggested that the high shear treatment provides homogeneous thermal and chemical fields, which resulted in a uniform distribution of potential nuclei, such as the magnesium oxide particles for the heterogeneous nucleation [21]. The high shear treatment was also demonstrated to improve the size distribution of potential nuclei so that the nucleation efficiency was enhanced [22]. In the present experiment, the high shear treatment plays a similar role in improving the spatial and size distribution of heterogeneous nucleation agents. These agents can be magnesium oxide particles, which exist inevitably in the melt and the reinforcing ceramic SiC particles which can act as potent nucleation sites [23,24].

At high magnification as shown in Figure 5, for the HS strip, individual SiC particles are largely seen to be dispersed randomly or uniformly in the matrix, although some are still in clusters consisted of a few or at most over ten particles (Fig. 5(a)). In contrast, SiC particles in the nonHS strip are largely agglomerated and the agglomeration contains hundreds to thousands of particles, leaving large volume of the material

depleted with SiC_p (Fig. 5(b)). This strongly suggests that the high shear treatment effectively dispersed the reinforcing SiC particles and that the agglomeration of particles during TRC was avoided, due to the provision of high cooling rate in the process.

Figure 6 shows the variation of the reinforcing particle volume fraction along the strip length for both the HS and nonHS strips. The average particle volume fraction was 5.2% and 5.0% for HS and nonHS, respectively, which are very close to the nominal value of 5%. However, the strong agglomeration of SiC particles in the nonHS strips led to large scattering of measured values through the strip thickness. The standard deviation of SiC particle volume fraction for nonHS strip was around 6 times higher than that for the HS strip. In order to evaluate the homogeneity of SiC particle distribution, Quadrat Method [25] was employed with 8×8 quadrat grid covering an area of 416 μm × 416 μm. More than 3500 SiC particles in 5 optical micrographs were counted for each sample. The Skewness β value [5], expressed by following equation:

$$\beta = \frac{q}{(q-1)(q-2)} \sum \left[\frac{N_{qi} - N_q^{mean}}{\sigma} \right]^3 \quad (1)$$

where q is the total number of quadrats studied, N_{qi} is the number of SiC particles in the ith quadrat (i= 1, 2, ……, q), N_q^{mean} is the mean number of SiC particles per quadrat, and σ is the standard deviation of the N_q distribution. The calculated Skewness β value of HS strip (Fig. 7) is lower at each measured points than the nonHS strip. A good consistency in β value was also obtained along 2000 mm long HS strip, which indicates improved particle distribution homogeneity at both the microscopic and macroscopic scales in the HS composite strip.

In the two-stage mixing process shown in Fig. 1, mechanical stirring with an impeller is responsible for the introduction of SiC particles into the melt with proper wetting and a

globally uniform distribution. Effective wetting between the particles and the molten alloy is expected to obtain via high shear treatment in the second stage of the mixing process. In the rotor stator device, the melt also undergoes two-stage treatment. Within the stator, the rotor rotates at a predetermined high speed and breaks down the particle agglomerations by the shear stress, generated between rotor and stator. The shear stress (τ) [26] can be estimated by the following equation:

$$\tau = \eta \frac{\pi N D}{\delta} \tag{2}$$

where η is the dynamic viscosity of composite melt, N is the rotating speed of the rotor head, D is the diameter of rotor head and δ is the gap between the rotor head and the inside surface of the stator. The viscosity η of AZ31/SiC_p slurry can be calculated by equation [27]:

$$\eta = \eta_0 \left(1 + \frac{5}{2}\varphi + \frac{109}{14}\varphi^2\right) \tag{3}$$

where η_0 is the dynamic viscosity of liquid phase, φ is the volume fraction of solid particles. Here for liquid AZ31, η_0 is about 1.23×10^{-3} Pa·s [28]. For the high shear mixing process, rotation speed is 5000 rpm. Combining Eq. (1) and (2) together, the shear stress on the composite melt is calculated to be ~ 450 Pa.

According to the Rumpf's model [29], the tensile strength T of an agglomeration of SiC particles can be estimated by following equation:

$$T = \frac{9}{32}\frac{\varphi}{\pi a^2} n_b F \tag{4}$$

where φ is the volume fraction of reinforcing particles with the radius of a, F is the average binding force of a single bond and n_b is the average number of bonds per particle (in nonHS sample of present study, $n_b$is 6 in average). Considering the particle-particle cohesive force from 5 nN to 15 nN of different ceramic particles in similar size

as of this study [30], the tensile strength of agglomerate can be calculated and found to be in the range of 6.5 ~ 19.5 Pa which less than 10^2 Pa. The shear stress provided by rotor-stator device is significantly higher than the strength for holding SiC agglomeration and can effectively break down the agglomerates. As the cluster tensile strength is inversely proportional to the square of particle size ($T \propto \frac{F}{a^2}$), the smaller the particle size, the higher the strength of the cluster. As the SiC particle size of reinforcement decreases, increased rotation speed of the rotor in the rotor-stator device is desirable to ensure a good dispersion of SiC_p.

At the same time, the high speed turbulent flow increases the contact between the particles and the melt and improves wetting between the alloy melt and the reinforcing particles, leading to the uniform dispersion of SiC_p within the AZ31 magnesium alloy melt. A special feature of the rotor stator device is the provision of apertures evenly distributed at the bottom part of the stator, through which the well mixed slurry is forced out. At this stage, the composite slurry undergoes the high shear stress due to the nature of friction generated from the viscous effect on the aperture wall through fluid squeezing and jetting out by high speed rotating rotor impeller. Once the slurry forced into the stator aperture, the slurry flow velocity decreases dramatically at the inner wall surface of aperture where the fluid dynamics changed. As a consequence large velocity gradient built up from boundary layer closing to the inner wall surface of the aperture to the centre of aperture hole where the shear stress applied on the composite slurry. The shear stress (τ) on the composite slurry through stator aperture can be presented by the following equation [31],

$$\tau = f\rho\vartheta^2/2 \tag{5}$$

where f is the flow friction factor which is 0.03 for turbulent in steel pipe (the Moody chart [31]), ρ is fluid density and ϑ is the mean flow velocity. The theoretical density of AZ31/5vol%SiC slurry is 1.72 g/cm^3 which calculated by rule of mixer and approximate flow velocity of slurry in similar rotor-stator mixer geometry and parameters is 10 m/s [19]. The shear stress of composite slurry experienced through a single stator aperture can be calculated as 2.6×10^3 Pa which further contributes to the particle dispersion by breaking up the particle agglomerations inside the apertures.

3.3 The effect of reinforcing particle on the matrix microstructure

Fig. 8 are the polarized light optical micrograph for both the HS and non HS composite strips, showing the differences in the primary a-Mg grain structures obtained from the different melt treatment schemes prior to TRC. The grain structure for the HS strip is uniform and fine with an average grain size of 39.3±14.9 μm. On the contrary, the nonHS strip showing an inhomogeneous grain structures with both coarse (above 100 μm) and fine grain of primary α-Mg phase, and the average grain size is 52.7±21.6 μm. The typical α-Mg grain size of majority of grains in the HS sample is in the range of 20 to 60 μm. For nonHS composites strip sample, grain size of primary α-Mg phase spread above 100 μm and more (Fig. 9).

Fig. 10 shows the microstructure inhomogeneity of nonHS sample with both the polarized and bright field micrographs. With absence of SiC particle observed in Fig. 10(a) and (c)), it is shown a coarse primary α-Mg with size about 120 μm, which was measured in the polarized micrograph. On the other hand, with the SiC particle agglomeration/cluster in Mg matrix (brighter contrast in Fig. 10(b) and dark contrast in Fig. 10(d)), a more refined microstructure was observed which is a typical microstructure of fine α-Mg grain. These microstructures suggest that the fine primary

α-Mg grains in the composite TRC strip is relating to the existence of SiC reinforcement as individual particle or small-sized agglomeration/cluster.

Fig. 11 shows the β-$Mg_{17}Al_2$ phase morphology with SiC distribution in the etched HS and nonHS strip samples. A clear α-Mg dendritic structure has been drawn out by the solute rich compounds emphasizing the interdendritic region in particle free area in the nonHS sample (Fig. 11(b)). On the contrary, the β-$Mg_{17}Al_{12}$ phase presented discretely in the HS sample with uniform distribution of SiC in Fig. 11(a). The further investigation of element distribution was carried out by EDS mapping. The α-Mg dendrites with long dendrite stem and large branch (indicated with white arrow) are shown in Fig. 11(d) with Al containing solute pushed to the interdendritic area forming coarse intermetallic phase. On the contrary, the network of interdendritic phase distributed uniformly accompanied with SiC particles well dispersed in the HS sample (Fig. 11(c)). The improved wetting between SiC and matrix AZ31 alloy can be seen in the HS strip as a certain portion of reinforcement particles exist inside the α-Mg dendrite rather than pushed to the interdendritic area [5] where latter solidified.

The uniform microstructure through the strip thickness and the elimination of solute segregations suggest that the solidification kinetics was significantly improved during TRC due to the high shear treatment. Combined with evidence above, the SiC could influence the solidification behaviour of AZ31 alloy in casting process. Previous research [32] also suggests that SiC particle as a potent nucleus for α-Mg heterogeneous nucleation due to small misfit of 2.3% with $(10\bar{1}0)_{Mg}//(0001)_{SiC}$ orientation relationship. Fine and uniform primary α-Mg grains in the AZ31/5vol%SiC_p HS sample in Fig. 8(a) could be explained as the heterogeneous nucleation enhanced by these well dispersed SiC particles which act as the potential nuclei during solidification of the strip. So that

nucleation took place evenly through strip thickness and equiaxed growth prevailed owing to uniform temperature and composition fields.

Such promotion of the enhanced nucleation sites in the HS sample by well dispersion of SiC particles also minimises the solute segregation through the composite strip. The SEM images of β-$Mg_{17}Al_{12}$ phase morphology and distribution are shown in Figure 12. In the HS sample, Al containing solute segregations, marked with white arrows, were located in the interdendritic area with major axis size less than 10 μm (Fig. 12(a) and (c)). In the case of the nonHS sample (Fig. 12(b) and (d)), $Mg_{17}Al_{12}$ lumps was coarser with size >20 μm in the major axis, and the number density of segregation compound significantly reduced. From the solidification sequence of AZ31 alloy [33], $Mg_{17}Al_{12}$ phase are expected to appear after the primary α-Mg formation from the melt. The size and distribution of primary α-Mg phase can determine the size and distribution of inter-grain area and further influence the solute segregation in the TRC process [20].

From the aspect of size and distribution, the primary α-Mg grain and $Mg_{17}Al_{12}$ phase in AZ31/5vol%SiC_p composite TRC strip are all influenced by the high shear dispersion of SiC_p during the solidification. Such a uniform microstructure and chemistry is important for the composite strip to display reliable mechanical and physiochemical performance.

3.4 Mechanical properties

3.4.1 Strength and ductility

The mechanical properties of the homogenized HS and nonHS composite TRC strips are presented in Figure 13. The yield and ultimate tensile strengths of the AZ31/5vol%SiC_p HS strips were observed to improve by 34.8% and 47.9% respectively, compared to that of the nonHS strips. The elongation is also improved from 2.3±0.6% to 3.0±0.3% by high shear dispersion. Figure 14 illustrates the SEM image of fracture

surface. Uniform and small sized dimples were observed on the fracture surface of the AZ31/5vol%SiC_p HS sample, whereas large α-Mg grain boundary and small dimples can be observed in sample without high shear treatment. Homogeneously distributed SiC particles resulted in uniform and small dimples in the HS sample, which denotes the ductile fracture behaviour. On the contrary, for the nonHS sample, large SiC agglomeration resulted in large voids, which contributing to the brittle fracture behaviour. Under tensile load, homogeneous distribution of the reinforcement particles contributes to uniform stress distribution and such well-bonded fine and hard SiC particles within AZ31 matrix behaving like precipitates enlarging the energy consumption for void formation, debonding or separation between the reinforcements and matrix [34]. On the other hand, in the nonHS samples the weaker bonding between SiC/SiC interfaces within SiC clusters, leads to development of cracks at lower loads and the failure occurs at early stage of the tensile force loading.

3.4.2 Hardness

The Vickers hardness of the AZ31/5vol%SiC_p HS and nonHS composite TRC strip samples are shown in Fig. 15. The average Vickers hardness values of the HS and nonHS samples are 86 Hv0.5 and 75 Hv0.5, respectively. The Vickers hardness values along three line scans through the strip thickness for the HS sample are in a narrow range (indicated with blue shade) between 74 Hv0.5 and 99 Hv0.5. On the contrary, in the nonHS sample, large fluctuations (red shade) observed, which reflects the inhomogeneous SiC_p distribution. In the region where SiC agglomeration is present, hardness as high as 120 Hv0.5 was observed. However, in the SiC particle free regions, a lower hardness of 45 Hv0.5 was shown. Hurricks [35] reviewed the metallurgical factors controlling the abrasive wear resistance of metallic materials and identified a

direct correlation between measured hardness and wear performance. To have superior wear performance, it is important to have minimal spatial variation of the hardness across the composite. Due to the observed homogeneous hardness in the HS strip, higher wear resistance is expected for the HS composite strip sample which can be attributed to improved SiC reinforcement distribution by high shear treatment.

3.4.3 Elastic modulus

Halpin-Tsai model [36], which predicts the modulus of particulate reinforcement composites with the assumption of homogeneous reinforcement distribution in the matrix, has been used to evaluate the elastic modulus of the homogenized HS and nonHS composite TRC strips. The elastic modulus of a composite is:

$$E_c = \frac{E_m(1+2sqV_p)}{1-qV_p} \tag{4}$$

where

$$q = \frac{(E_p/E_m-1)}{(E_p/E_m)+2s} \tag{5}$$

and E_c, E_m and E_p are the elastic modulus of the composite, matrix and particle, respectively, E_m of 42.31 GPa is obtained through experimental measurement of AZ31 strip with same processing route as composite TRC strips, E_p of 450 GPa [37] is employed due to the similar manufacturing condition of silicon carbide particles used in this work. V_p is the volume fraction of particle, and s is the particle aspect ratio. Since SiC particle morphology used in this study is angular, s is measured to be 1.5 and 3 for lower and upper limits. The comparison of elastic modulus prediction and experimental measurement is presented in the Figure 16. It can be seen that the measured elastic modulus for the HS sample is in agreement with the model predicted range but the nonHS composite TRC strip sample significantly deviated. In general, the volume

fraction of reinforcement is the dominant factor that controls the elastic modulus. However, in the similar volume fraction condition as in the case of the HS and nonHS, particle spatial distribution significantly influences the elastic modulus. Non-uniform distribution of the reinforcement leads to the non-uniform stress distribution in the material and may cause the reduction in the modulus [38]. The measured elastic modulus of the AZ31/5vol%SiC_p nonHS composite deviated from the theoretical calculation due to the presence of large SiC agglomeration and particle free areas. In the case of the AZ31/5vol%SiC_p HS composite TRC strip, the measured elastic modulus is in good agreement with the Halpin-Tsai model due to homogeneous distribution of SiC particles.

4. Conclusion

1. A two stage process for processing composite slurry involving conventional mechanical stirring followed by the rotor-stator high shear treatment has been developed for producing magnesium alloy matrix particulate reinforcing composites slurry, and has been successfully used in the production of AZ31/5vol%SiC_p composite strips by twin roll casting.
2. The composite strip exhibited a fine microstructure for the matrix alloy with a uniform distribution of SiC particles, and enhanced modulus, yield strength and ductility, compared to that produced without high shear treatment.
3. The uniform temperature and chemical fields generated by the high shear treatment was responsible for the uniform microstructure through the thickness of the strip and global uniform particle distribution. The high shear rate and high shear stress provided by the rotor-stator device broke up particle agglomeration and led to the formation of particle dispersion.

4. SiC particles are considered to act as heterogeneous nucleation sites for α-Mg, contributing to the observed grain refinement. The high cooling rate in the twin roll casting process contributed partly to the grain refinement for the matrix alloy and global uniform distribution of particles as well.

Acknowledgement

This work is supported by EPSRC UK, Towards Affordable, Close-Loop Recyclable Future Low Carbon Vehicle Structures (TARF-LCV), Grant No. EP/I038616/1. Author would like to thank Dr Hu-Tian Li, Mr Peter Lloyd and Mr Graham Mitchell for their experimental support for TRC process and Dr Hari-Babu Nadendla for technical discussion at BCAST, Brunel University London.

Reference

1. Fleming S. An Overview of Magnesium based Alloys for Aerospace and Automotive Applications. Dissertation for Master Degree, Rensselaer Polytechnic Institute, New York 2012.

2. Sasaki TT, Oh-ishi K, Ohkubo T, Hono K. Effect of double aging and microalloying on the age hardening behavior of a Mg–Sn–Zn alloy. Mater Sci Eng: A 2011;530:1-8.

3. Bhattacharjee T, Mendis CL, Sasaki TT, Ohkubo T, Hono K. Effect of Zr addition on the precipitation in Mg–Zn-based alloy. Scr Mater 2012;67(12):967-970.

4. Jiao Y, Zhang J, Jing Y, Xu C, Liu S, Zhang L, Xu L, Zhang M, Wu R. Development of High-Performance Mg Alloy via Introducing Profuse Long Period Stacking Ordered Phase and Stacking Faults. Adv Eng Mater 2015;17(6):876-884.

5. Lloyd D. Particle reinforced aluminium and magnesium matrix composites. Int Mater Rev 1994;39(1):1-23.

6. Tjong SC. Novel Nanoparticle-Reinforced Metal Matrix Composites with Enhanced Mechanical Properties. Adv Eng Mater 2007;9(8):639-652.

7. Dieringa H. Properties of magnesium alloys reinforced with nanoparticles and carbon nanotubes: a review. J Mater Sci 2011;46(2):289-306.

8. Lenel FV. Powder Metallurgy: Principles and Applications. : Metal Powder Industry, 1980.

9. Hashim J, Looney L, Hashmi MSJ. Particle distribution in cast metal matrix composites—Part I. J Mater Process Technol 2002;123(2):251-257.

10. Barekar N, Tzamtzis S, Babu NH, Fan Z, Dhindaw B. Processing of ultrafine-size particulate metal matrix composites by advanced shear technology. Metal Mater Trans A 2009;40(3):691-701.

11. Hashim J, Looney L, Hashmi MSJ. Particle distribution in cast metal matrix composites—Part II. J Mater Process Technol 2002;123(2):258-263.

12. Fan ZY, Zuo YB, Jiang B, A new technology for treating liquid metals with intensive melt shearing. In: Mater Sci Forum. , 2011. p. 141-144.

13. Patel J, Zuo Y, Fan Z, Krane M, Jardy A, Williamson R, Beaman J, Liquid metal engineering by application of intensive melt shearing. In: Proceedings of the 2013 International Symposium on Liquid Metal Processing and Casting, TMS 2013. , 2013. p. 291-299.

14. Hansen S, Khakhar D, Ottino J. Dispersion of solids in nonhomogeneous viscous flows. Chem Eng Sci 1998;53(10):1803-1817.

15. Rohatgi P, Asthana R, Das S. Solidification, structures, and properties of cast metal-ceramic particle composites. Int Metal Rev 1986;31(1):115-139.

16. Park SS, Bae G, Kang D, You B, Kim NJ. Superplastic deformation behavior of twin-roll cast Mg–6Zn–1Mn–1Al alloy. Scr Mater 2009;61(2):223-226.

17. Karnezis P, Durrant G, Cantor B, Palmiere E. Mechanical properties and microstructure of twin roll cast Al–7Si/SiCp MMCs. Mater Sci Tech 1995;11(8):741-752.

18. Li J, Huang Y, Microstructure and mechanical properties of an Mg-3Zn-0.5Zr-5HA nanocomposite processed by ECAE. In: IOP Conference Series: Mater Sci Eng. , 2014. p. 012112.

19. Utomo A, Baker M, Pacek A. The effect of stator geometry on the flow pattern and energy dissipation rate in a rotor–stator mixer. Chem Eng Res Design 2009;87(4):533-542.

20. Barekar N, Dhindaw B. Twin-roll casting of aluminum alloys–An overview. Mater Manuf Process 2014;29(6):651-661.

21. Fan Z, Wang Y, Xia M, Arumuganathar S. Enhanced heterogeneous nucleation in AZ91D alloy by intensive melt shearing. Acta Mater 2009;57(16):4891-4901.

22. Men H, Jiang B, Fan Z. Mechanisms of grain refinement by intensive shearing of AZ91 alloy melt. Acta Mater 2010;58(19):6526-6534.

23. Günther R, Hartig C, Bormann R. Grain refinement of AZ31 by (SiC)P: Theoretical calculation and experiment. Acta Mater 2006;54(20):5591-5597.

24. Lelito J, Zak PL, Shirzadi AA, Greer AL, Krajewski WK, Suchy JS, Haberl K, Schumacher P. Effect of SiC reinforcement particles on the grain density in a magnesium-based metal–matrix composite: Modelling and experiment. Acta Mater 2012;60(6–7):2950-2958.

25. Tzamtzis S, Barekar N, Babu NH, Patel J, Dhindaw B, Fan Z. Processing of advanced Al/SiC particulate metal matrix composites under intensive shearing–A novel Rheo-process. Compos Part A Appl Sci Manuf 2009;40(2):144-151.

26. Atiemo-Obeng VA, Calabrese RV. Rotor–stator mixing devices. Handbook of industrial mixing: Science and practice:479-505.

27. Guth E, Simha R. Untersuchungen über die Viskosität von Suspensionen und Lösungen. 3. Über die Viskosität von Kugelsuspensionen. Colloid Polym Sci 1936;74(3):266-275.

28. Culpin M. The viscosity of liquid magnesium and liquid calcium. Proc Phys Soc Sec B 1957;70(11):1079.

29. Rumpf H. The strength of granules and agglomerates. In: Knepper WA, editor. Agglomeration. New York, U. S. A.: Wiley, 1962. p. 379-418.

30. Jones R, Pollock HM, Geldart D, Verlinden A. Inter-particle forces in cohesive powders studied by AFM: effects of relative humidity, particle size and wall adhesion. Powder Technol 2003;132(2–3):196-210.

31. Douglas JF, Gasiorek JM, Swaffield JA, Jack LB. Fluid Mechanics Sixth Edition. Essex: Pearson Education Limited, 2011.

32. Cai Y, Taplin D, Tan MJ, Zhou W. Nucleation phenomenon in SiC particulate reinforced magnesium composite. Scr Mater 1999;41(9):967-971.

33. Laser T, Nürnberg MR, Janz A, Hartig C, Letzig D, Schmid-Fetzer R, Bormann R. The influence of manganese on the microstructure and mechanical properties of AZ31 gravity die cast alloys. Acta Mater 2006;54(11):3033-3041.

34. Sreekumar V, Babu NH, Eskin D, Fan Z. Structure–property analysis of in-situ Al–MgAl 2 O 4 metal matrix composites synthesized using ultrasonic cavitation. Mater Sci Eng: A 2015;628:30-40.

35. Hurricks PL. Some metallurgical factors controlling the adhesive and abrasive wear resistance of steels. A review. Wear 1973;26(3):285-304.

36. Halpin JC. In: Anonymous Primer on Composite Materials: Analysis. Lancaster, PA: Technomic Publ, 1984. p. 130.

37. Wolfenden A, Oliver KA, Singh M. Measurements of elastic and anelastic properties of reaction-formed silicon carbide ceramics. J Mater Sci 1996;31:6073-6076.

38. Wang Z, Chen T, Lloyd D. Stress distribution in particulate-reinforced metal-matrix composites subjected to external load. Metal Trans A 1993;24(1):197-207.

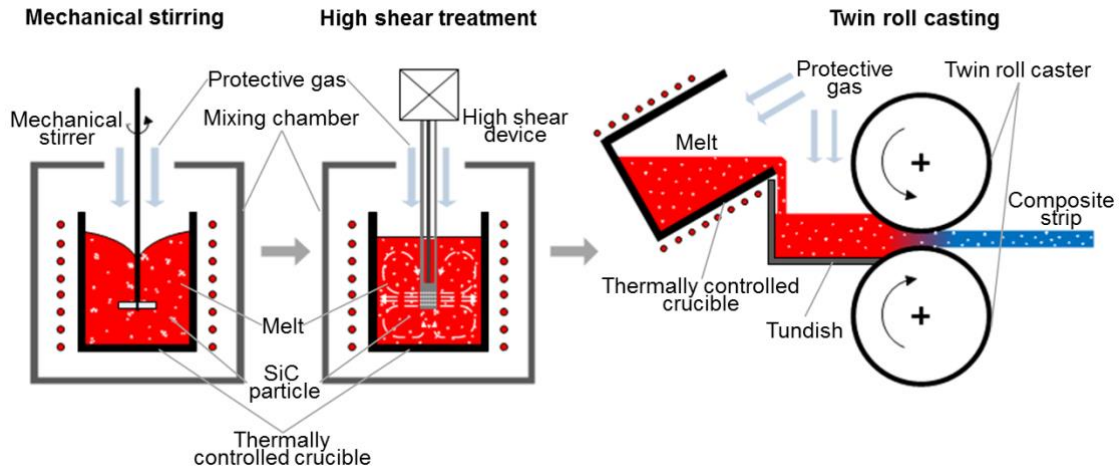

Figure 1. The schematic of SiC particle reinforced AZ31 magnesium matrix composite strip casting process involving a two-stage mixing process and the TRC process.

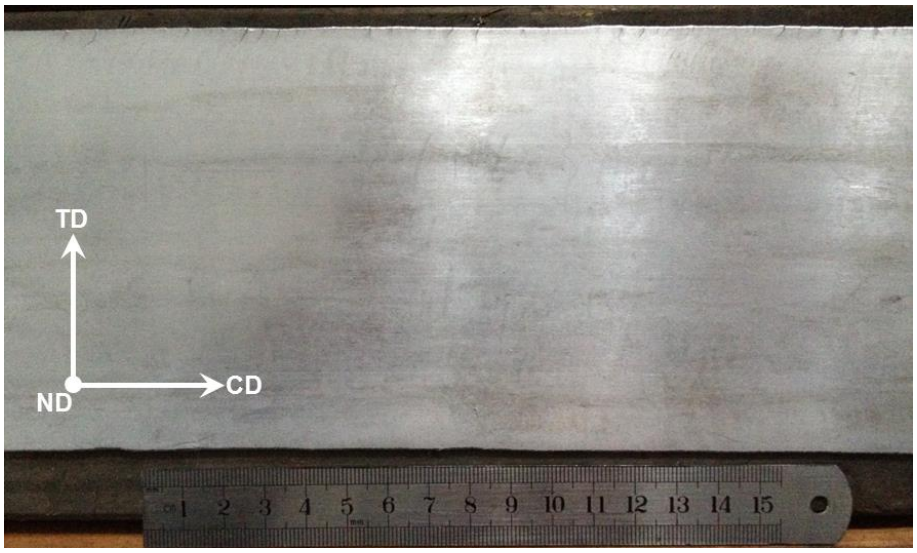

Figure 2. A photograph of AZ31/5vol%SiC_p composite strip.

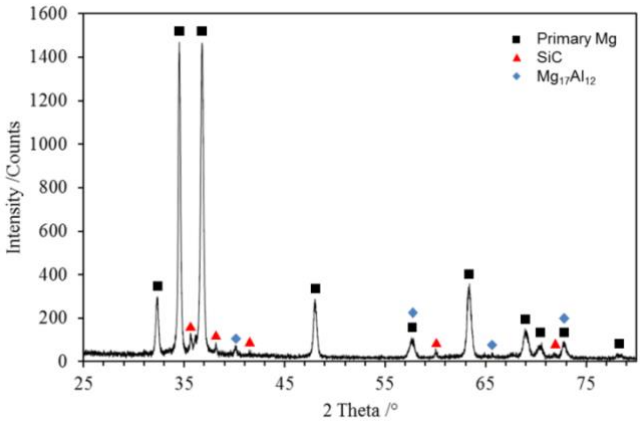

Figure 3. The XRD pattern of the strip fabricated from high shear treated AZ31/5vol%SiC_p slurry.

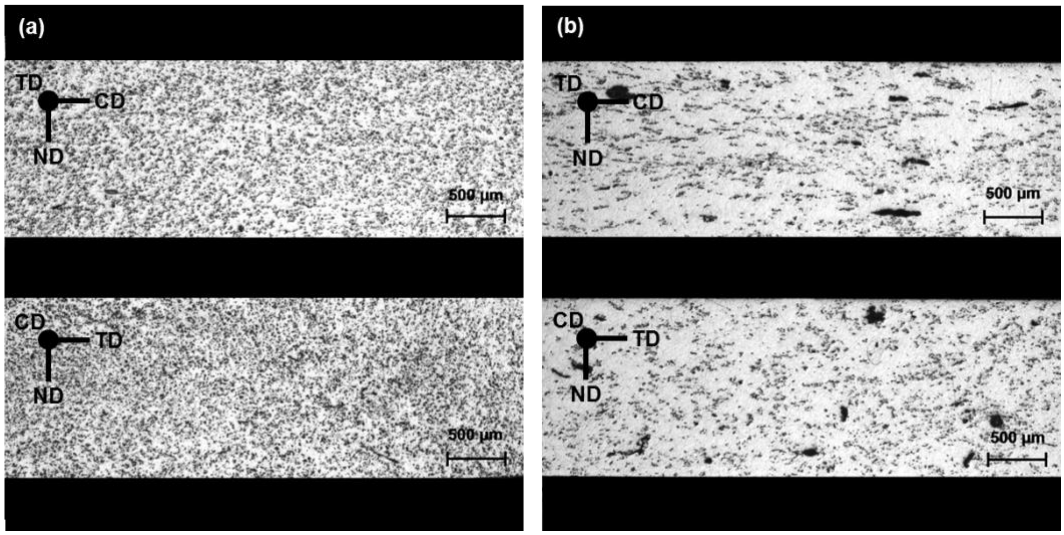

Figure 4. The longitudinal section and transverse section view of AZ31/5vol%SiC_p composite TRC strip fabricated with (a) high shear treatment clearly displaying the uniform distribution of SiC_p, and (b) without high shear treatment showing a number of agglomerates.

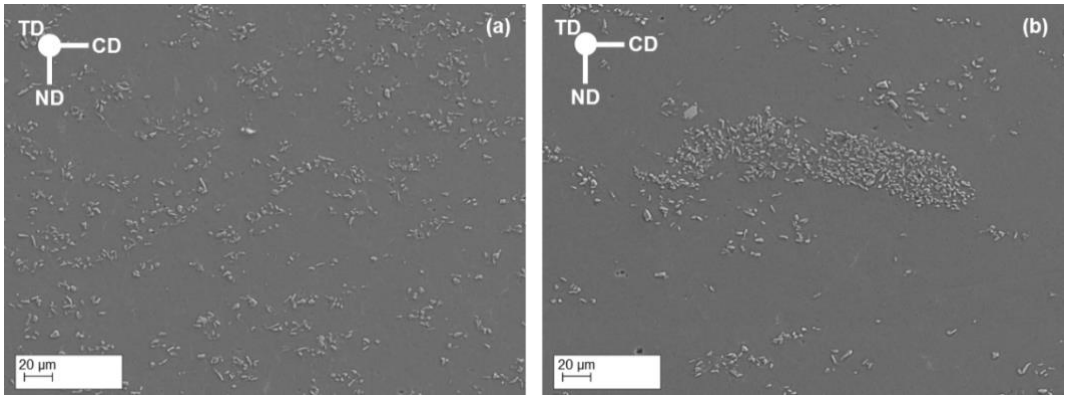

Figure 5. SEM image of the longitudinal section view of AZ31/5vol%SiC_p composite TRC strip fabricated (a) with high shear treatment and (b) without high shear treatment. A large sized cluster is clearly visible in the nonHS strip sample.

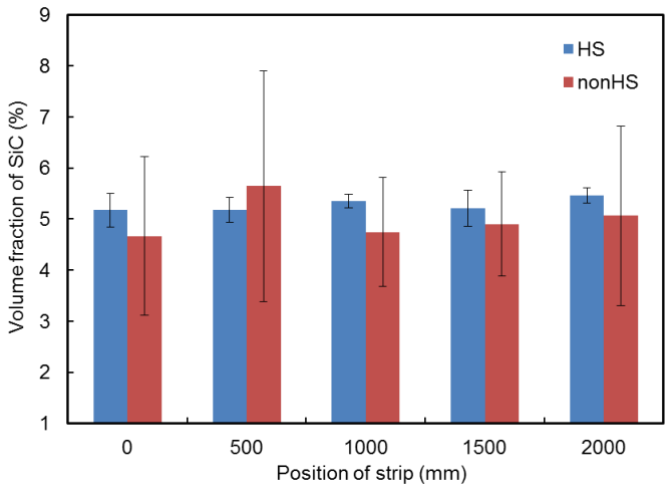

Figure 6. Spatial variation of the volume fraction of SiC particles in the longitudinal section of AZ31/5vol%SiC_p composite TRC strip fabricated with high shear treatment (HS) and without high shear treatment (nonHS). The obtained results demonstrate the efficiency of the high shear treatment for the particle distribution.

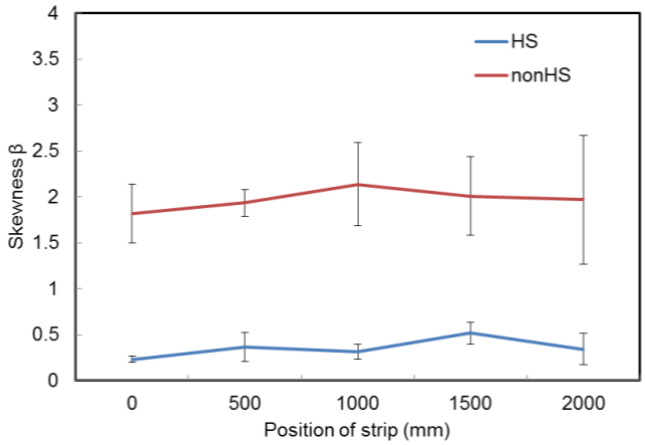

Figure 7. The distribution of reinforcing particles (Skewness β) determined by quadrat method in the longitudinal section of AZ31/5vol%SiC_p composite TRC strip fabricated with high shear treatment (HS) and without high shear treatment (nonHS) at different positions along the strip. Higher β values indicate severe agglomeration in the nonHS strip.

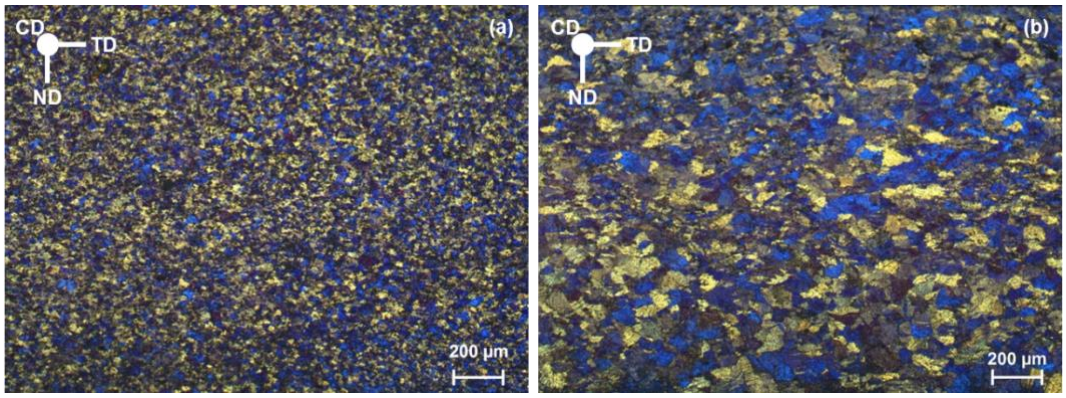

Figure 8. Polarised optical microscopy images of the transverse section of AZ31/5vol%SiC_p composite TRC strip fabricated (a) with high shear treatment and (b) without high shear treatment. Refinement in the grain size is evident in the HS strip.

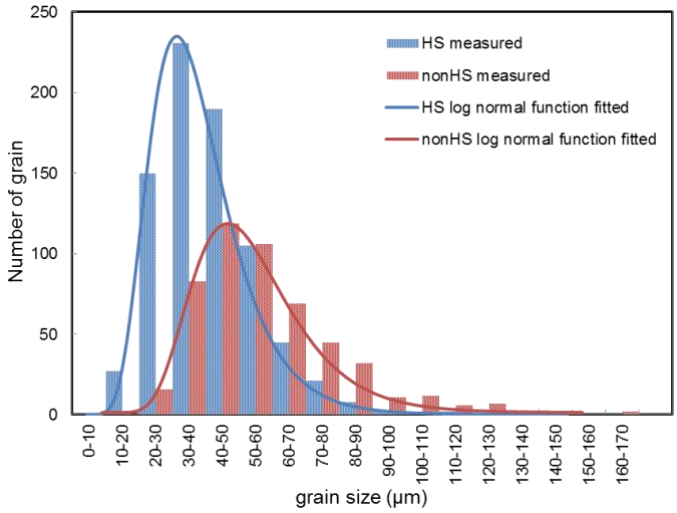

Figure 9. The primary α-Mg grain size distribution in the transverse section of AZ31/5vol%SiC_p composite TRC strip fabricated with high shear treatment (HS) and without high shear treatment (nonHS). The high shear treatment has resulted in narrower grain size distribution.

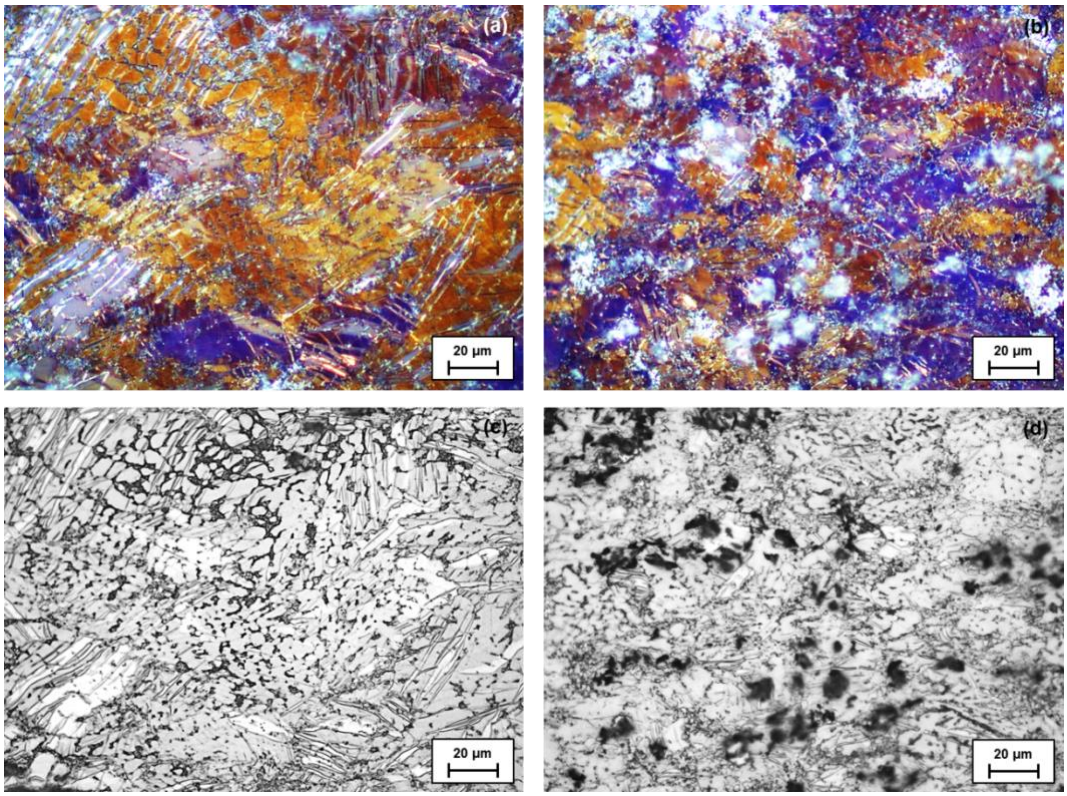

Figure 10. The polarized and bright field microstructure of the nonHS composite strip in the particle free area (a) and (c), and SiC cluster area (b) and (d), respectively.

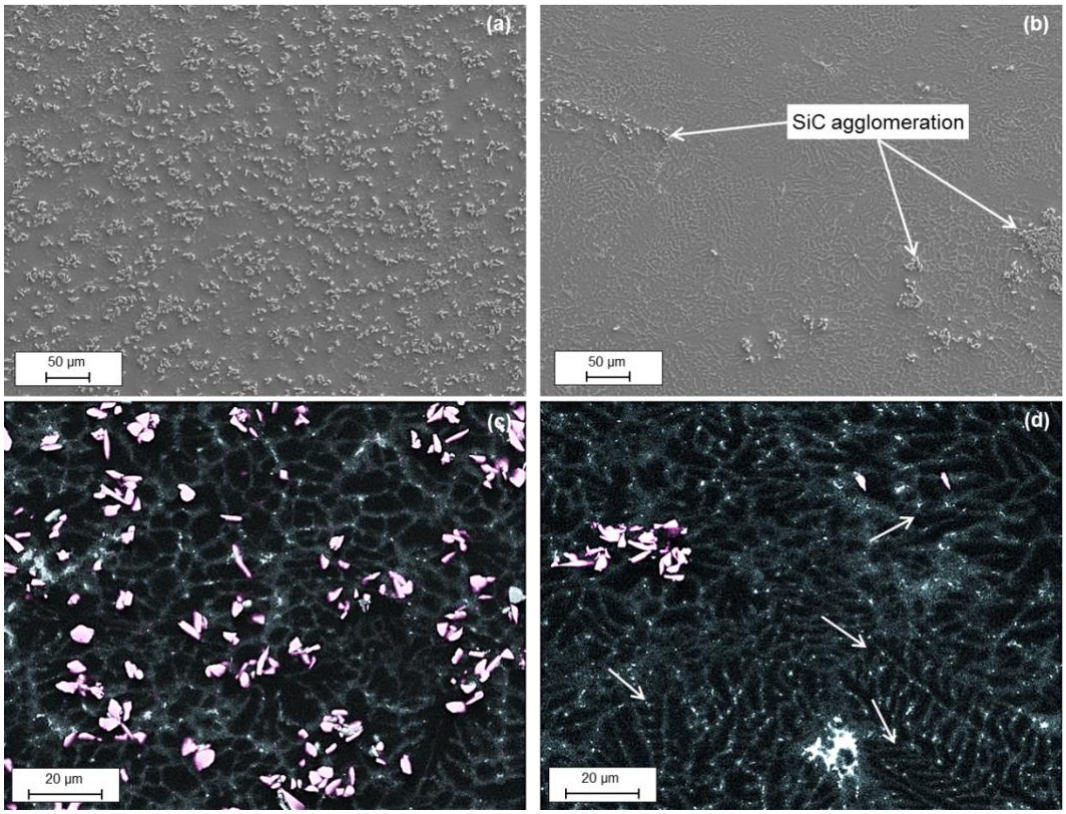

Figure 11. SEM image and the EDS mapping (Si and Al elements overlap) of the AZ31/5vol%SiC_p composite TRC strip fabricated with high shear treatment (a) and (c), and without high shear treatment (b) and (d), respectively. The bright pink contrast represents Si element on EDS mapping and dilute white contrast represent Al element in the composite TRC sample, respectively.

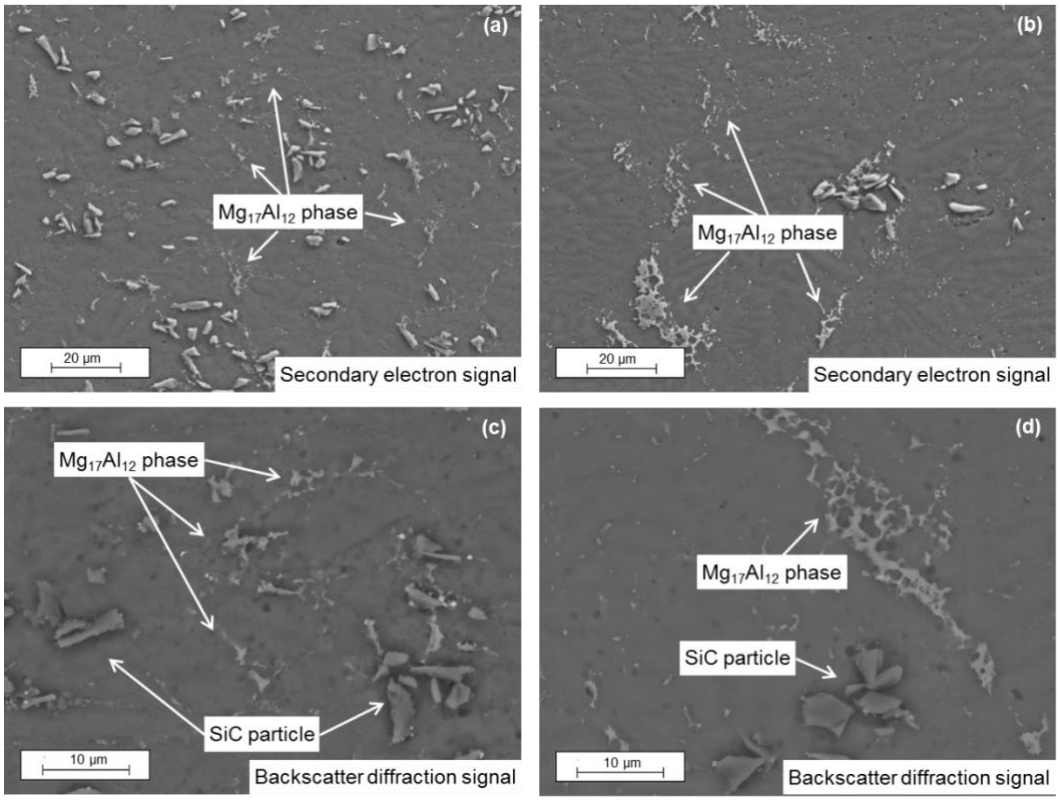

Figure 12. SEM image of the β-$Mg_{17}Al_{12}$ segregation of AZ31/5vol%SiC_p composite TRC strip fabricated with high shear treatment (a) and (c), and without high shear treatment (b) and (d).

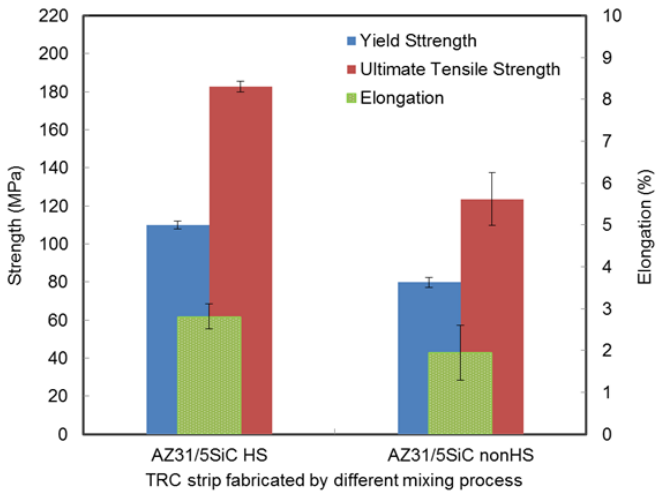

Figure 13. The mechanical properties of the AZ31/5vol%SiC_p composite TRC strip fabricated with high shear treatment (HS) and without high shear treatment (nonHS).

Compared to those produced without high shear treatment, the HS samples have a much improved tensile strength and ductility.

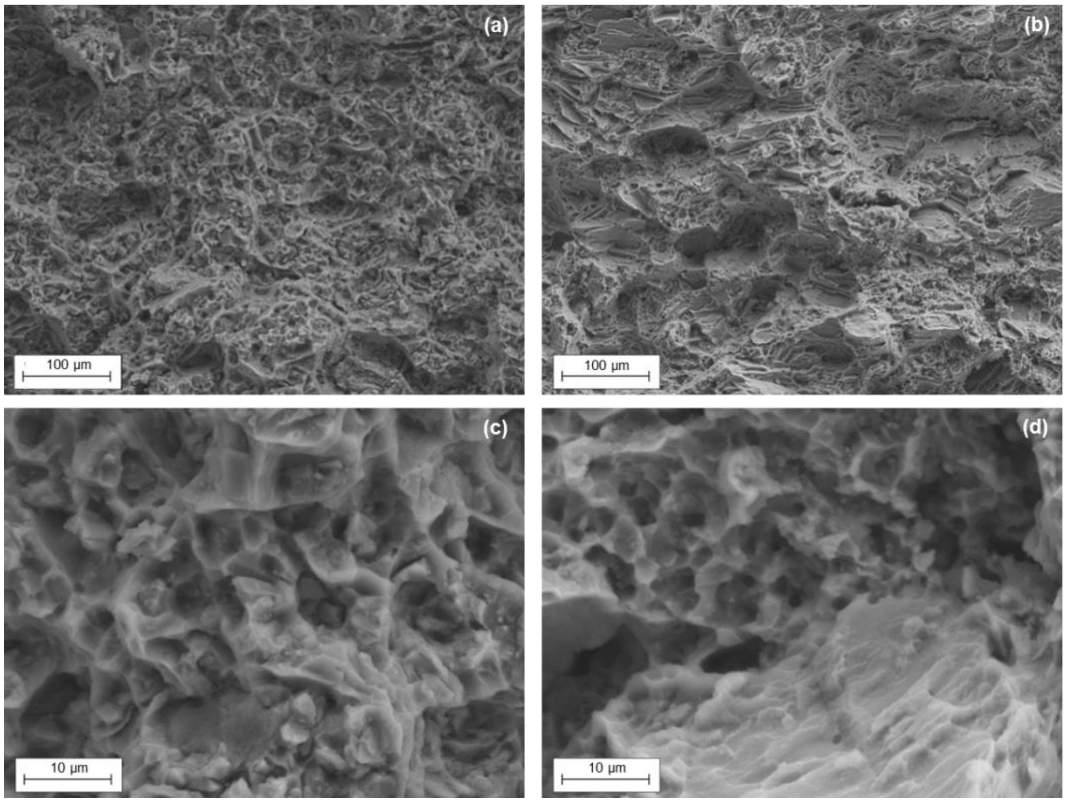

Figure 14. SEM image of the tensile fracture of the AZ31/5vol%SiC_p composite TRC strip fabricated with high shear treatment (a) and (c), and without high shear treatment (b) and (d).

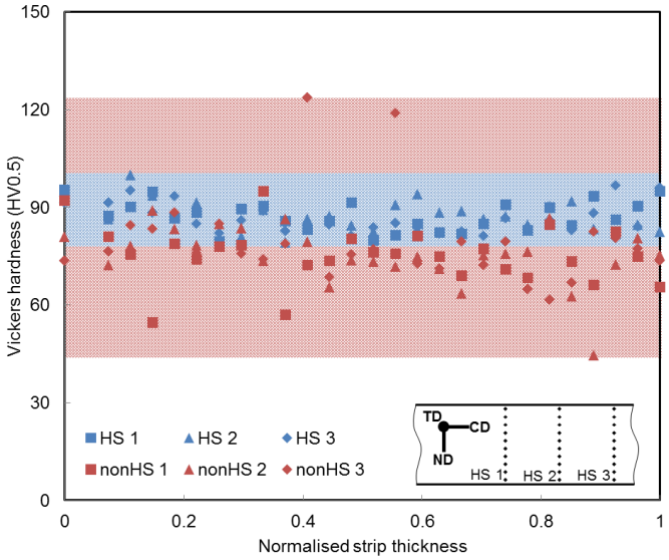

Figure 15. The Vickers hardness of the AZ31/5vol%SiC_p composite TRC strip fabricated with high shear treatment (HS) and without high shear treatment (nonHS). Inset shows a sketch of three line scans of HV indentation locations. Less scattering of the hardness values was observed for the HS strip.

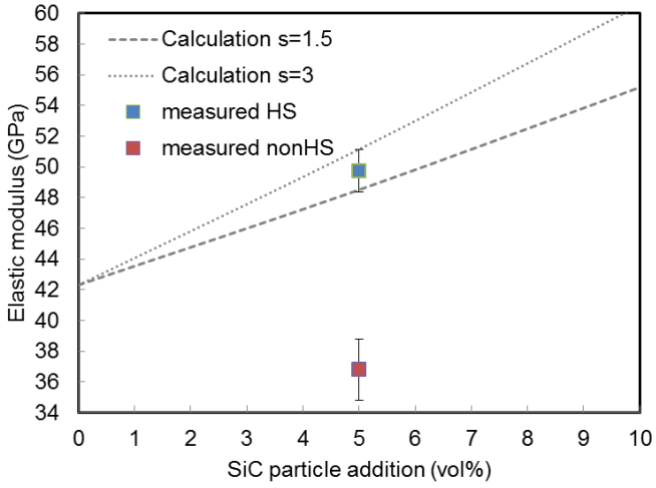

Figure 16. The predicted modulus as a function of reinforcement concentration by Halpin-Tsai model with two different particulate aspect ratios. Measured elastic modulus of the AZ31/5vol%SiC_p composite TRC strip with high shear treatment (HS) and without high shear treatment (nonHS) are also shown for comparison.